Available online at www.sciencedirect.com
SCIENCE DIRECT®
Journal of Sound and Vibration 294 (2006) 162–176
JOURNAL OF SOUND AND VIBRATION
www.elsevier.com/locate/jsvi

Active automotive engine vibration isolation using feedback control

Claes Olsson*

Volvo Car Corporation, Chassis & Vehicle Dynamics, Department 96260, PVH34 405 31 Gothenburg, Sweden

Received 4 February 2005; received in revised form 27 October 2005; accepted 31 October 2005
Available online 5 January 2006

Abstract

Large frequency band feedback active automotive engine vibration isolation is considered. A MIMO (multi-input multi-output) controller design for an active engine suspension system has been performed making use of a virtual development environment for design, analysis, and co-simulation based closed-loop verification. Utilising relevant control object dynamic modelling, this design strategy provides a powerful opportunity to deal with various plant dynamics, such as structural flexibility and nonlinear characteristics where the main objective is to approach the actual physical characteristics for design and verification in early design phases where no prototypes are yet physically available.

$\mathscr{H}_2$ loop shaping technique proves to be powerful when achieving the desired frequency dependent loop gain while ensuring closed-loop stability. However, to achieve closed-loop stability two kinds of nonlinearities have to be taken into account. Those are nonlinear material characteristics of the engine mounts and large angular engine displacements. It is demonstrated how the adopted design strategy facilitates the investigation of the latter nonlinearity's impact on closed-loop characteristics. To deal with the nonlinearities, gain scheduling has been used.

1. Introduction

Reducing structure borne noise and vibration induced by, for instance, engines, through reducing vibrations at the disturbance source, is one of the main objectives of engine suspension systems. Many papers have been published on development of such systems using active engine mounts; one of the earliest is that by McDonald et al. [1]. They describe a MIMO active engine vibration isolation system using the *multiple error LMS* (*least mean square*) *algorithm* [2–4].

The LMS algorithm and a similar one referred to as the *filtered-x LMS algorithm* [5] are by far the most common approaches when dealing with narrow band vibration isolation [6,7]. Although it seems to be more difficult to find literature on automotive engine vibration isolation systems based on feedback control [8], it has been applied to other applications. Watters, Coleman, Duckworth, and Bukman describe a SISO system for large frequency band active vibration isolation of a marine engine [9]. Other examples on feedback active vibration isolation systems are given in Refs. [10–12].

*Tel.: +46(0)31 3251310; fax: +46(0)31 590730.
E-mail address: colsson5@volvocars.com.

0022-460X/$ - see front matter © 2005 Elsevier Ltd. All rights reserved.
doi:10.1016/j.jsv.2005.10.022

When attenuating transmitted forces over a broad-band of frequencies, a feedforward approach has to utilise a multitude of narrow band filters which slows down the speed of convergence. Furthermore, these filters have to be continuously adapted when the spectral content of the excitation is changing with time. Since, in contrast to feedback control, the performance of a feedforward controller is very sensitive to errors in the phase of the control filters, this could lead to poor performance.

Turning to broad-band feedback control, the design relies very much on the quality of the model of the control object and the main concern is to achieve closed-loop stability. The design of a feedback controller is more intricate than the design of a feedforward controller, but it gives design control over the loop gain, and consequently ability to design to performance specification and to provide reasonable closed-loop stability guarantees. It is also possible to estimate and consequently avoid excessive measurement noise amplification outside the desired bandwidth.

In this paper, model-based controller design is adopted where the plant model for controller synthesis is transferred from a multibody system analysis and simulation environment to the controller design one. Controller synthesis is then followed by verification using closed-loop *co-simulation* where the two software packages are run concurrently: one simulating the control system functionality, and another predicting the response of the plant during various disturbances. This procedure constitutes a design strategy that aims to approach the actual dynamical characteristics for design and virtual verification in early design phases where no physical prototypes are available. It should be compared with the more traditional ones based on system identification or analytical equations of motion.

The objective is to investigate the potential of MIMO feedback control for broad-band vibration isolation of a car engine suspended using rubber mounts with nonlinear material characteristics, while making use of the above mentioned design strategy.

The organisation of the contents is as follows: Sections 2 and 3 describe the plant and the operating conditions to be considered, while the design specifications are given in Section 4. Section 5 presents an $\mathscr{H}_2$ controller design based on a linearised plant model. The final design steps are presented in Sections 6 and 7 where the effects of nonlinearity and input saturation are considered. Finally, Section 8 presents some concluding remarks.

2. Plant description

The considered engine is a three point suspended 5-cylinder combustion diesel engine that is attached to the vehicle body at LHS (left-hand side) and RHS (right-hand side) via two rubber engine mounts. Furthermore, it is also connected to the subframe via a TR (torque rod) with rubber bushings at both ends, see Fig. 1. The engine suspension system has to support the engine at static equilibrium state, prevent large movements due to transient and low frequency road disturbances, and isolate engine dynamic vibration generated by engine and road disturbances for different gearing ratios in the whole range of engine rotational speed.

To deal with this problem in a proper way, it is essential to have an accurate model of the physical system (engine, engine suspension, receiver, and excitation) that comprises its frequency characteristics, its nonlinearity, and its physical properties variation, and is available all the time for control strategy analysis, development, and verification in time domain. This will have a large impact on controller synthesis, performance, and stability verifications.

A virtual environment consisting of two different software packages have been used for physical modelling of the engine and its suspension system, control system modelling and design of controller, and virtual verification of outcomes, i.e. control algorithms. They are

- a multibody system analysis and simulation software for dynamics (ADAMS) [13],
- a real-time analysis and simulation software for control synthesis (Matlab/Simulink).

This environment for closed-loop time-domain simulation, analysis, and verification, has the advantage of accurate and time efficient managing of large physical models, broad-band frequency characteristics, flexible structures, nonlinear physical systems, generation of linearised equations of motion, synthesis and analysis of control algorithms, general input/output relationship.

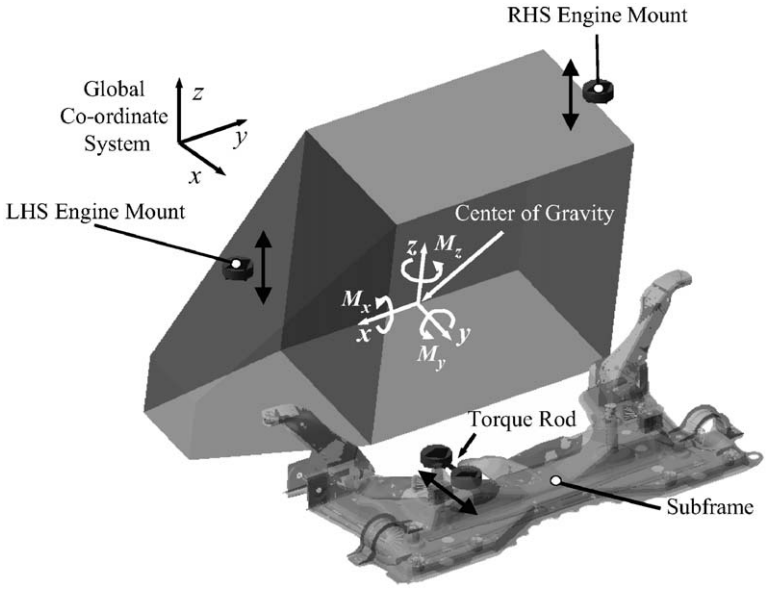

Fig. 1. Engine model with engine suspension layout, its connection to body and subframe, its local, and the global vehicle coordinate system. The bidirectional arrows indicate plant input and output directions, i.e. directions of control forces and directions of force measurements.

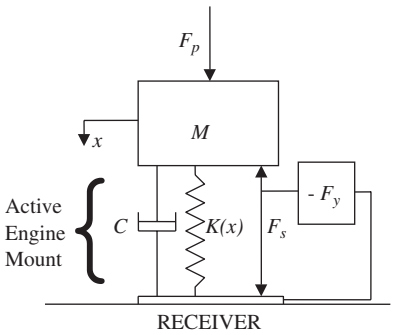

Fig. 2. Schematic picture of the principle of operation of the active engine mounts.

Making use of the multibody system analysis and simulation software package [13], the engine and torque rod are modelled using rigid body representation, giving an analysis model with 12 kinematical dofs (degrees of freedoms). The engine mounts at left- and right-hand side of the engine, as well as the bushings connecting the torque rod to the engine and the subframe are modelled using 6dofs (three translational and three rotational) spring and damper elements with non-linear stiffness, linear damping characteristics, and clamped free ends. Thus, the body and subframe attachment points are regarded as rigid in all directions.

In addition to the passive suspension system, three controllable forces are introduced in parallel with LHS and RHS mounts, and torque rod rear bushing. These are the plant inputs with directions according to Fig. 1. More specifically, the plant inputs are two forces that act in z-direction (with respect to the global vehicle coordinate system) in parallel to the LHS and RHS engine mounts, and a force that acts in the longitudinal direction of the torque rod in parallel to its rear bushing. The plant outputs are the total resultant transmitted forces (i.e. the sum of the plant inputs and the forces in the passive mounts) in the three clamped suspension points, in the direction of the plant inputs. In practice, the force inputs together with the 6dofs stiffness and damping elements are integrated into one unit called an *active engine mount*. For any one of the three active engine mounts, Fig. 2 shows schematically the principle of operation when only the degree of freedom

corresponding to the direction of the plant input (and output) is considered. In reality, the plant inputs could be generated by e.g. electrodynamic actuators. In Fig. 2, F_s is the plant input, $K(x)$ and C represent the stiffness and damping in the direction of the plant input. M and F_p correspond to engine mass and engine disturbance, respectively. F_y is the controller feeding back the plant output (i.e. the total force transmitted to the receiver) according to

$$\Sigma F(t) = K(x)x(t) + C\dot{x}(t) + F_s(t). \tag{1}$$

At and above idle frequency the engine is subjected to internal disturbances, originating from rotating and translating masses and firing gas forces which has been calculated from measured cylinder pressure curves, specific engine loads (torque applied to breaks during gas pressure measurements), and inertial properties of engine parts. These disturbances are described by the three fluctuating torques M_x, M_y, and M_z, with respect to the engine coordinate system (see Fig. 1), applied to the engine centre of gravity.

3. Engine operating conditions

The internal engine disturbance is mainly order based. This means that for a specific engine speed, the spectral content of the disturbance contains frequency components at frequencies equal to multiples of the rotational engine speed. For convenience the letter "E" is often used where E is the rotational speed of the engine in Hz. The ignition frequency, i.e. the frequency component at 2.5 times the rotational speed is hence referred to as $2.5E$ and, furthermore, the ith order at N rev/min fulfils the relation $f = N \cdot i/60$, where f is the frequency in Hz.

Dealing with the internal engine disturbance, two load cases have been used which give rise to principally different responses, they are

- the idle operating condition of the specific engine at 700 rev/min,
- the driving operating condition during a rotational speed 4 s sweep from 700 rev/min, i.e. idling, to 5000 rev/min. This corresponds to an acceleration of the car causing a torque applied to the engine block. This torque consists of a nominal torque depending on several parameters such as gear ratio and weight of the car and a fluctuating torque superimposed on the nominal one. Fig. 3 shows the frequency contents of the internal fluctuating torque M_x, for various rotational engine speeds. The magnitudes correspond to maximum cylinder pressure.

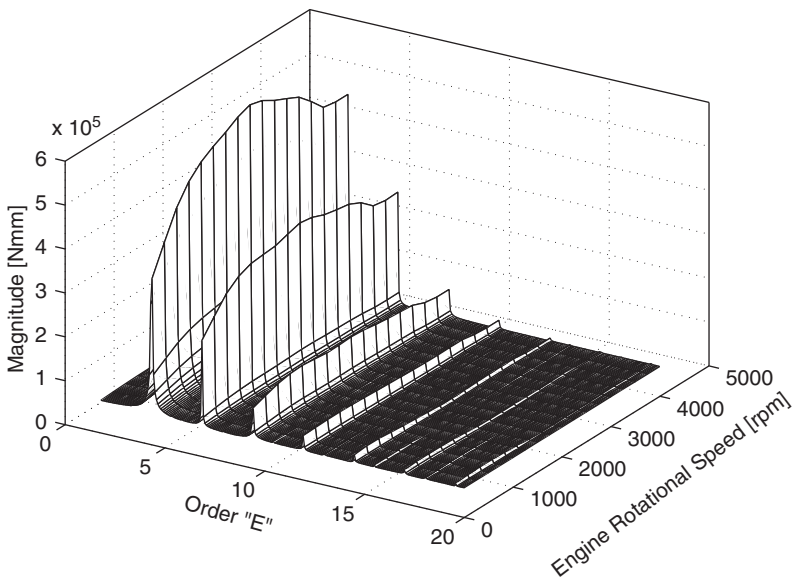

Fig. 3. Spectral frequency content of the combustion fluctuating torque M_x, for various rotational engine speeds and maximum load.

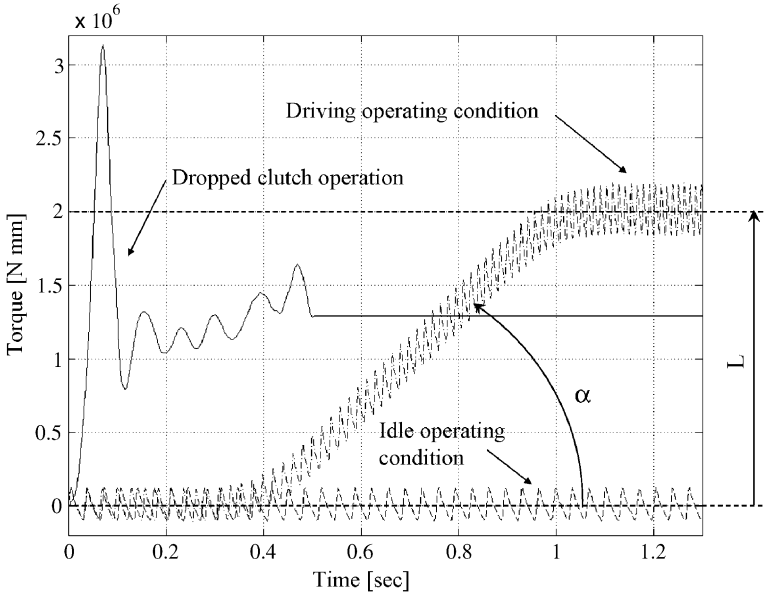

Fig. 4. Measured 1st gear engine torque during a dropped–clutch operation and the torque, M_x, corresponding to engine idle operating conditions and to an acceleration of the car. L and α represent nominal torque level and ramping speed, respectively.

To evaluate the ability of the controller to deal with high load transient disturbance, the resulting drive torque on the engine block due to a dropped–clutch operation has been measured. This disturbance characteristics, called "Shunt and Shuffle", is shown in Fig. 4 together with a time history of the resulting torque, M_x, corresponding to idle operating condition and an acceleration of the car, including both nominal and fluctuating torque.

4. Plant dynamics and design specification

Based on *Lagrange equations of motion*, a first order differential equation is derived which could be generally written as

$$\begin{aligned} \dot{\mathbf{x}} &= f(\mathbf{x}, \mathbf{u}, \mathbf{m}), \\ \mathbf{z} &= h(\mathbf{x}, \mathbf{u}, \mathbf{m}), \end{aligned} \tag{2}$$

where $\mathbf{x}$ is a column vector of internal states, $\mathbf{u}$ is the plant control input, $\mathbf{m}$ is the plant disturbance excitation, and $\mathbf{z}$ is the plant output. Eq. (2) is automatically linearised [14] around static equilibrium position which leaves a minimal state space realisation according to (3) which is imported into Matlab and used for controller synthesis.

$$\begin{aligned} \dot{\mathbf{x}} &= \mathbf{A}\mathbf{x} + \mathbf{B}\mathbf{u} + \mathbf{N}\mathbf{m}, \\ \mathbf{z} &= \mathbf{C}\mathbf{x} + \mathbf{D}\mathbf{u}. \end{aligned} \tag{3}$$

In Eq. (3), $\mathbf{u}$ and $\mathbf{z}$ are plant inputs and outputs, respectively, and $\mathbf{m} = [M_x \;\; M_y \;\; M_z]^{\mathrm{T}}$ (see Fig. 1). Since the plant model has 12 kinematical degrees of freedom, the dimension of the state $\mathbf{x}$ is 24 while $\mathbf{m}$, $\mathbf{u}$, and $\mathbf{z}$ are all 3×1 vectors. Including sensor noise $\mathbf{n}$ in the measurement $\mathbf{y}$ of the plant output $\mathbf{z}$, the linearised plant representation (3), could also be written as

$$\begin{aligned} \mathbf{z} &= \mathbf{G}(s)\mathbf{u} + \mathbf{w}, \\ \mathbf{y} &= \mathbf{z} + \mathbf{n}, \end{aligned} \tag{4}$$

with

$$\mathbf{G}(s) = \mathbf{C}(s\mathbf{I} - \mathbf{A})^{-1}\mathbf{B} + \mathbf{D}, \tag{5}$$

where $\mathbf{w}$ represents the internal engine and external road disturbances transformed to the output of the system. Introducing the linear negative feedback controller $\mathbf{F}_y(s)$ according to

$$\mathbf{u} = -\mathbf{F}_y(s)\mathbf{y} \tag{6}$$

and inserting Eq. (6) into Eq. (4) gives the following relations for the closed-loop system:

$$\begin{aligned} \mathbf{z} &= \mathbf{S}(s)\mathbf{w} - \mathbf{T}(s)\mathbf{n}, \\ \mathbf{u} &= \mathbf{T}_{uw}(s)(\mathbf{w} + \mathbf{n}). \end{aligned} \tag{7}$$

Here $\mathbf{S}(s)$ is the sensitivity function [15] defined as

$$\mathbf{S}(s) = (\mathbf{I} + \mathbf{G}(s)\mathbf{F}_y(s))^{-1} \tag{8}$$

and $\mathbf{T}(s)$ is the complementary sensitivity function [15] denoted as

$$\mathbf{T}(s) = (\mathbf{I} + \mathbf{G}(s)\mathbf{F}_y(s))^{-1}\mathbf{G}(s)\mathbf{F}_y(s). \tag{9}$$

Furthermore, the output of the controller due to $\mathbf{w}$ is determined by the transfer function from $\mathbf{w}$ to $\mathbf{u}$, here denoted $\mathbf{T}_{uw}(s)$ where

$$\mathbf{T}_{uw}(s) = -\mathbf{F}_y(s)(\mathbf{I} + \mathbf{G}(s)\mathbf{F}_y(s))^{-1}. \tag{10}$$

It is desirable to deal with engine disturbance order one up to, and including, order five. Therefore, considering the engine rotational speed range (700–5000 rev/min), vibration isolation is wanted from approximately 12 to 420 Hz. Moreover, the low frequency characteristics of the original passive suspension have to be preserved (i.e. no control action below 12 Hz) maintaining the ability to prevent large engine displacements, e.g. due to transient disturbance and high level nominal loads. These closed-loop requirements could be summarised in terms of the singular values of:

(R1) $\mathbf{S}(s)$, determining the disturbance attenuation. As typically for band-limited disturbance attenuation, the singular values of $\mathbf{S}(s)$ should be very small in the frequency range where attenuation is wanted, i.e. from approximately 12 Hz to about 420 Hz. Outside this frequency region, $\mathbf{S}(s)$ should ideally be equal to one which implies no control action (i.e. zero open-loop gain).

(R2) $\mathbf{T}(s)$, determining the propagation of sensor noise and degree of robust stability with respect to model uncertainties. These should ideally be small everywhere and, most importantly, they have to be small for high frequencies where the signal-to-noise ratio is low.

(R3) $\mathbf{T}_{uw}(s)$, determining the necessary control power. This requirement emerges from the fact that actuators and power sources are limited and that there should be no control action below 12 Hz. Therefore, it is desirable with small singular values of $\mathbf{T}_{uw}(s)$ for all frequencies but especially for frequencies below $1E$ at idle engine operation.

Considering the singular values of $\mathbf{G}(s)$ and the closed-loop requirements, it is straightforward to express these in terms of open-loop gain requirements, visualised in Fig. 5 (superimposed on the singular values of $\mathbf{G}(s)$). Fig. 5 also defines, for convenience, frequency ranges I–III, to be referred to throughout this paper. From Fig. 5 it is clear that the requirements put on the open-loop gain, are not realistic. For example, the sharp transitions between the different frequency regions are not possible without a very high order controller. As mentioned earlier, there is also a trade-off between attenuation of disturbance (from road and engine) and measurement noise propagation (since $\mathbf{S}(s) + \mathbf{T}(s) = \mathbf{I}$). Moreover, if the largest singular value of $\mathbf{S}(s)$ is less than one in some frequency range it must be larger than one elsewhere [16]. The model of the engine (3) contains two zeros in the RHP, i.e. a so-called non-minimum phase system implying even stronger limitations on $\mathbf{S}(s)$ (see, for instance, Refs. [15] and [16]).

In Section 2, it was mentioned that body and subframe are modelled as rigid bodies. In view of the frequency range considered (see Fig. 5), it is clear that this is not a valid assumption. Even if the choice of force feedback rather than e.g. acceleration minimises the degree to which modal flexibility couples into the feedback loop [9,10], this has to be regarded as a limitation and a topic for future investigations.

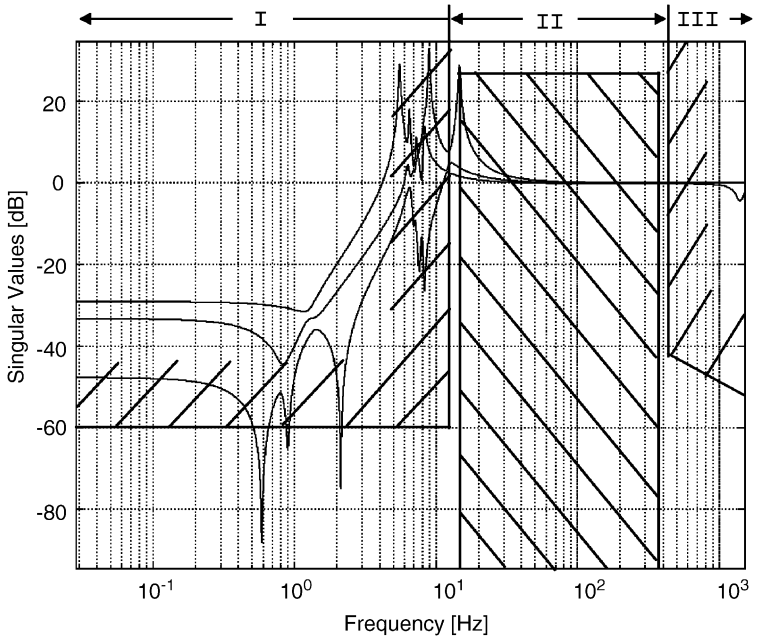

Fig. 5. The ideal requirements on the singular values of the open-loop gain, $\mathbf{G}(s)\mathbf{F}_y(s)$, ▨ = forbidden area.

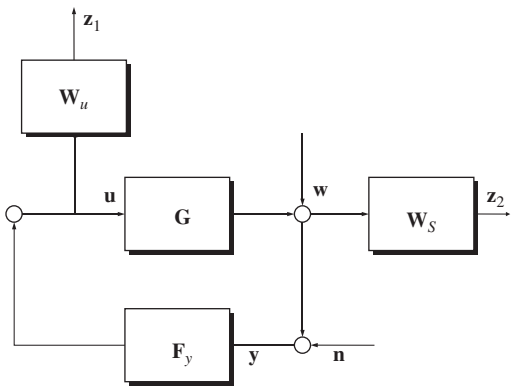

Fig. 6. Feedback configuration with weighting functions for $\mathscr{H}_2$ synthesis.

5. $\mathscr{H}_2$ control of the linearised plant

$\mathscr{H}_2$ controller synthesis is the process of choosing a feedback controller in order to minimise the $\mathscr{H}_2$-norm of some frequency weighted closed-loop transfer function. Specifically, minimising the $\mathscr{H}_2$-norm of the transfer function from $\mathbf{w}$ to $\mathbf{z}$ ($\mathbf{z} = [\mathbf{z}_1\ \mathbf{z}_2]^{\mathrm{T}}$, a 6×1 vector) in Fig. 6 over every $\mathbf{F}_y(s)$ means that the following norm is minimised:

$$\|\mathbf{T}_{zw}(s)\|_2^2 = \left\| \begin{bmatrix} \mathbf{W}_u(s)\mathbf{T}_{uw}(s) \\ \mathbf{W}_S(s)\mathbf{S}(s) \end{bmatrix} \right\|_2^2, \tag{11}$$

where the $\mathscr{H}_2$ norm of a matrix function $\mathbf{F}(s)$ is defined as

$$\|\mathbf{F}(s)\|_2^2 = \frac{1}{2\pi}\int_{-\infty}^{\infty} \mathrm{Tr}[\mathbf{F}^*(\mathrm{j}\omega)\mathbf{F}(\mathrm{j}\omega)]\,\mathrm{d}\omega. \tag{12}$$

The weighting functions for $\mathbf{S}(s)$ and $\mathbf{T}_{uw}(s)$ are chosen to reflect the closed-loop design specifications.

5.1. $\mathscr{H}_2$ synthesis

Design and validation of a $\mathscr{H}_2$ [16,15] controller is first carried out based on the linearisation (3) of the nonlinear object. To reflect the design requirements on $\mathbf{S}(s)$ in frequency region II, a dynamic weighting function $\mathbf{W}_S(s)$ with high gain in this region is chosen. Well clustered singular values of the closed-loop quantities is achieved using diagonal weighting functions with the same SISO dynamic filter for each channel. In addition to a weighting function $\mathbf{W}_S(s)$, a weighting function $\mathbf{W}_u(s)$ has to be introduced in order to decrease the levels of the singular values of $\mathbf{T}_{uw}(s)$ in frequency region I. The transfer functions of the weighting functions are chosen to be

$$\mathbf{W}_u(s) = \frac{10^2(1+s/(2\pi))^2(1+s/(2\pi 300))}{(1+s/(2\pi\cdot 0.03))^2(1+s/(2\pi 10^4))}\cdot\mathbf{I}, \tag{13}$$

$$\mathbf{W}_S(s) = \frac{w_{s1}(s)\cdot w_{s2}(s)}{1+s/(2\pi 10^4)}\cdot\mathbf{I}, \tag{14}$$

where

$$w_{s1}(s) = \frac{10.924(s^2+87s+(2\pi\cdot 11)^2)^3}{(s^2+110s+(2\pi\cdot 16.5)^2)^3}, \tag{15}$$

$$w_{s2}(s) = \frac{(s^2+5000s+(2\pi\cdot 500)^2)^3}{11\cdot(s^2+3000s+(2\pi\cdot 333)^2)^3}. \tag{16}$$

In the transfer function expression for $\mathbf{W}_S(s)$, $\omega_{s1}(s)$ and $\omega_{s2}(s)$ are designed to force the sensitivity to be small in frequency region II while the term in the denominator guarantees existence of the norm $\|\mathbf{W}_S(s)\mathbf{S}(s)\|_2^2$. The precise form for $\omega_{s1}(s)$ and $\omega_{s2}(s)$ asserts rapid transitions of the loop gain between the frequency regions in agreement with Fig. 5. The terms in the transfer function expression for $\mathbf{W}_u(s)$ are basically chosen to force the gain of $\mathbf{T}_{uw}(s)$ to be small in frequency region I. The term $(1+s/(2\pi 10^4))$ in the denominator counteracts the equal term in the expression for $\mathbf{W}_S(s)$.

The sensitivity and the complementary sensitivity corresponding to the chosen weighting functions $\mathbf{W}_u(s)$ and $\mathbf{W}_S(s)$ are shown in Fig. 7. This figure reveals that the controller provides about 20 dB attenuation in the frequency range from approximately 16 to 250 Hz, more than 10 dB attenuation between 250 and 500 Hz, and also that the total forces transmitted to the body and subframe may be amplified by approximately 4 dB, i.e. with a factor of 1.6, for frequencies between 1 and 8 Hz. The design trade-off at frequencies near 10 Hz was expected and is mainly due the design requirement on the open-loop gain to have a sharp transition between frequency regions I and II.

6. Control of the non-linear plant

Using $\mathscr{H}_2$ control theory guarantees stability even though the stability margins could be arbitrarily small [17]. Furthermore, differences between the model used for controller design and the true physical plant, might lead to performance degradation. For this particular problem, the linear model previously used for design in Section 5 is known to have modelling errors due to linearisation. Therefore, it should be evaluated with respect to the original model using closed-loop time domain simulations. This is carried out using the principle of *co-simulation* schematically described in Fig. 8 where ADAMS and Matlab solvers are run concurrently, one simulating the control system functionality, and another predicting the response of the plant.

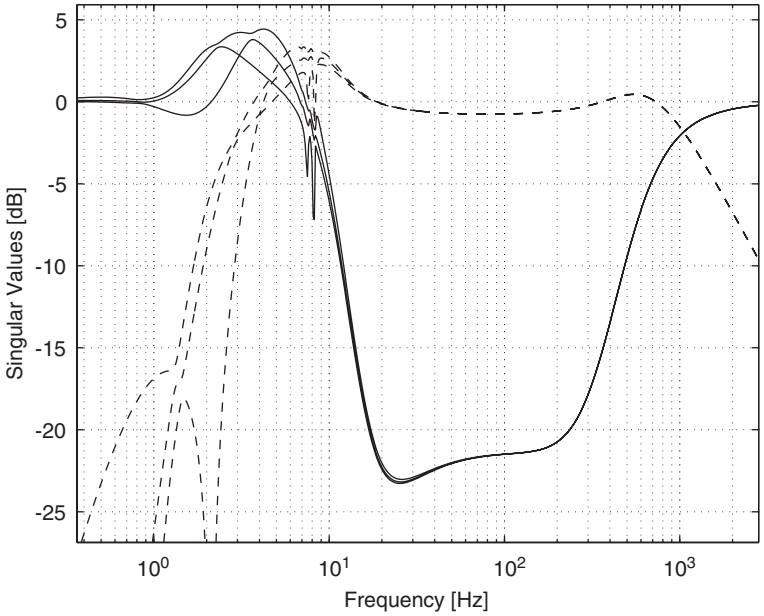

Fig. 7. $\mathbf{S}(s)$ (solid) and $\mathbf{T}(s)$ (dashed) for a design with trade-off made between good low and good high closed-loop frequency characteristics.

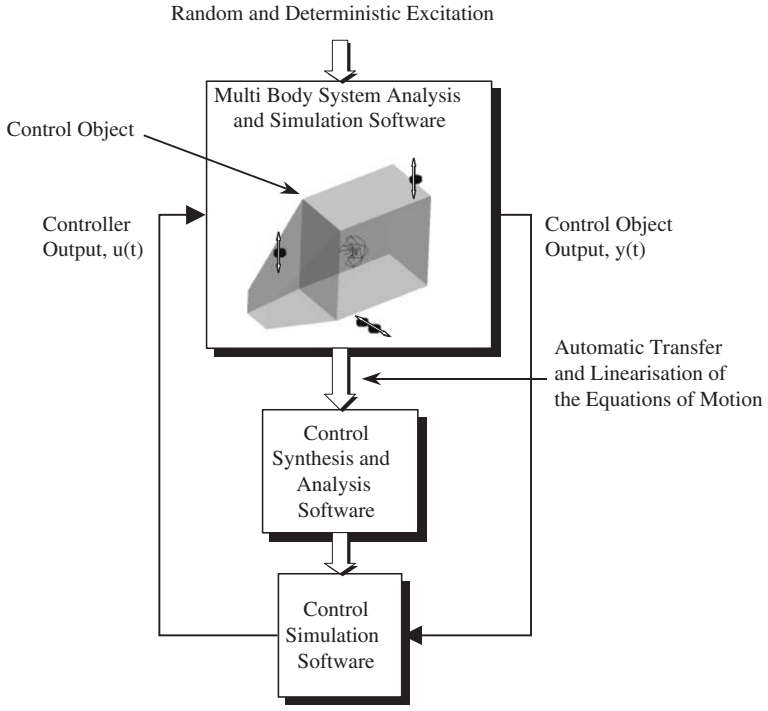

Fig. 8. Analysis, closed-loop co-simulation, and verification environment.

6.1. Gain scheduling control

Co-simulations bring forward that even for moderate nominal levels of the torque M_x, causing mount and bushing forces well within the linear stiffness ranges (see Appendix, Section A.2), there is closed-loop

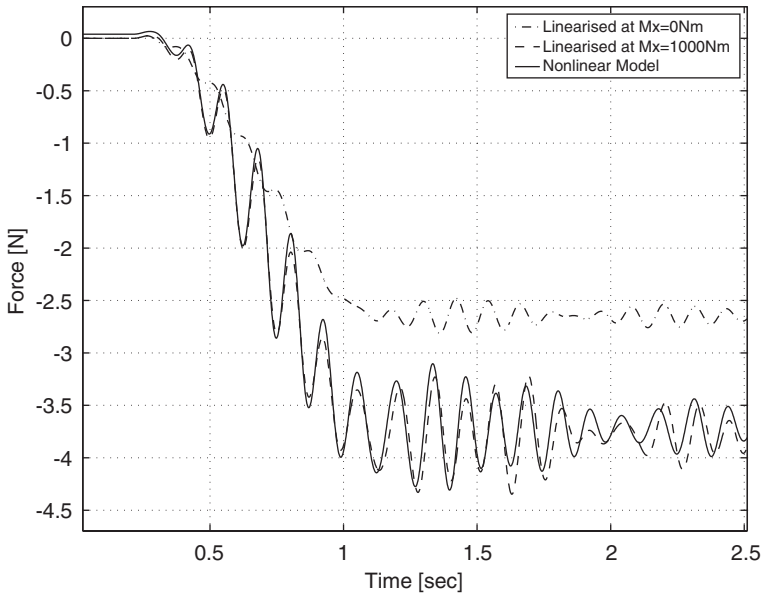

Fig. 9. Transmitted force at RHS corresponding to the nonlinear model (solid), a linearisation at $M_x = 0\,\mathrm{N\,m}$ (dash-dotted), and a linearisation at $M_x = 1000\,\mathrm{N\,m}$ (dashed), when subjected to a nominal torque from 1000 to 1050 N m.

instability when using the controller developed in Section 5. The reason for this phenomenon is clear from Fig. 9, presenting results from open-loop simulations where the nonlinear plant and two linearisations around two different levels of the nominal part of the torque M_x (see Fig. 1), $M_x = 0\,\mathrm{N\,m}$ and $M_x = 1000\,\mathrm{N\,m}$, have been subjected to M_x equal to a ramp from 1000 to 1050 N m. Since in these simulations, the mount and bushing forces are within the linear stiffness ranges, the graph illustrates the effects of nonlinearity due to large angular displacements. Apparently, the plant exhibits two different kinds of nonlinear behaviours. These are nonlinear material characteristics of the mounts and bushings, and large angular engine displacements. In both cases, the nonlinear behaviour depends on the level of the nominal part of the torque M_x.

The problem of instability has been solved using *gain scheduling* [18]. The controller is based on linearisations around four different equilibrium operating points described by the nominal level m_e of the torque M_x, represented as

$$\begin{aligned} \delta\dot{\mathbf{x}} &= \mathbf{A}(m_e)\delta\mathbf{x} + \mathbf{B}(m_e)\mathbf{u} + \mathbf{N}(m_e)\delta\mathbf{m}, \\ \delta\mathbf{z} &= \mathbf{C}(m_e)\delta\mathbf{x} + \mathbf{D}(m_e)\mathbf{u}, \end{aligned} \tag{17}$$

where $\delta\mathbf{x} = \mathbf{x} - \mathbf{x}_e$, $\delta\mathbf{m} = \mathbf{m} - \mathbf{m}_e$, $\delta\mathbf{z} = \mathbf{z} - \mathbf{z}_e$, $\mathbf{m} = [M_x \;\; M_y \;\; M_z]^{\mathrm{T}}$, and $\mathbf{m}_e = [m_e \;\; 0 \;\; 0]^{\mathrm{T}}$.

The final controller consists of four $\mathscr{H}_2$ controllers based on linearisations around $m_e = 0$, 500, 1000, and 1500 N m, with linearly interpolated controller parameters. The parameter used for scheduling is the force transmitted to the body at LHS in the global x-direction which approximately obeys a linear relation to the nominal level of M_x. This requires an extra force sensor while measurements or calculations of the nominal level of M_x could be avoided.

Gain scheduling requires a scheduling parameter accurately describing the equilibrium operating point of the nonlinear plant. Since the force used for scheduling has to be low pass filtered, it cannot reflect the operating point for rapidly changing plant dynamic characteristics. This is the case when the engine is subjected to high load disturbance causing the plant to exhibit nonlinear material characteristics or when the nominal level of the M_x-torque changes rapidly. Considering Fig. 4, illustrating the three main disturbance characteristics, this means that gain scheduling is limited to those load cases corresponding to low

and moderate levels of the two parameters α and L, representing ramping speed and nominal torque level, respectively. High values of α means deteriorated performance, while high L-values could potentially imply closed-loop instability. In practice, the controller has to be switched off for these extreme load cases.

6.2. Controller order reduction

As a consequence of the specific closed-loop design specifications presented in Section 4, the realisation of the controller designed in Section 5.1 requires 72 states. These are 39 states from the weighting function $\mathbf{W}_S(s)$, 9 states from $\mathbf{W}_u(s)$, and 24 states from the linear model of the plant. A potential limitation of the gain scheduling approach is that the parameters of the different controllers must have same structure so that they could be linearly interpolated. Therefore, many controller reduction procedures implying state reordering, cannot be used. However, using balanced realisation and truncation of both the engine suspension model and the weighting functions before synthesising the $\mathscr{H}_2$ controllers, the final controller could be reduced to an order of 38, with preserved performance and stability. Considering the desired shape of the open-loop gain with the sharp transition between frequency region I and II and the many natural modes of the plant close to 10 Hz, see Fig. 5, this required number of states is not surprising.

7. Simulations

The gain scheduled $\mathscr{H}_2$ controllers described above have been evaluated using co-simulation. Both for disturbances corresponding to idle and various driving operating condition with moderate nominal load levels, the performance is in accordance with the sensitivity presented in Fig. 7.

Fig. 10 demonstrates the excellent performance when the engine is subjected to excitation corresponding to idle engine operating condition, while Fig. 11 presents the results of a simulation where the disturbance corresponds to a 4 s engine rotational sweep from 700 to 5000 rev/min, demonstrating the ability to deal with time varying disturbance (varying rpm and varying nominal torque level) in the whole speed range.

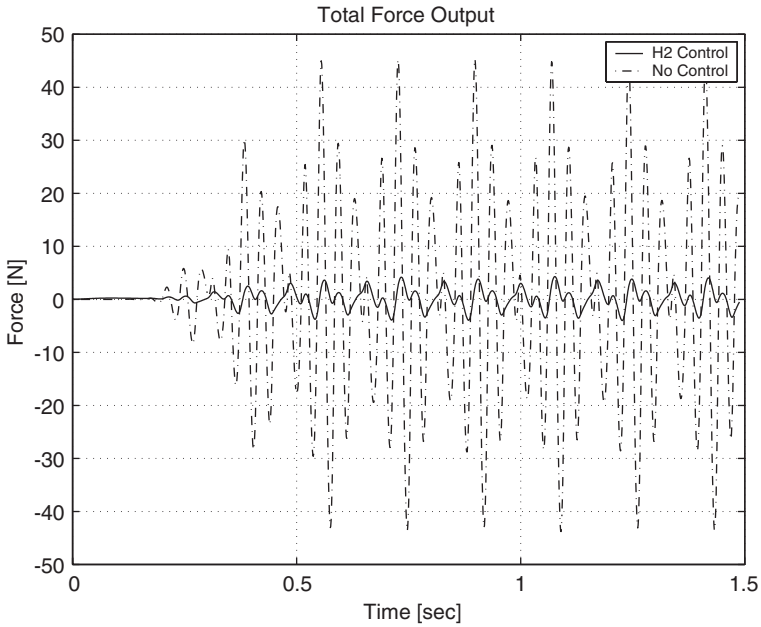

Fig. 10. Total transmitted force at RHS, with (solid) and without control (dash-dotted). The engine is subjected to excitation corresponding to idle operating condition.

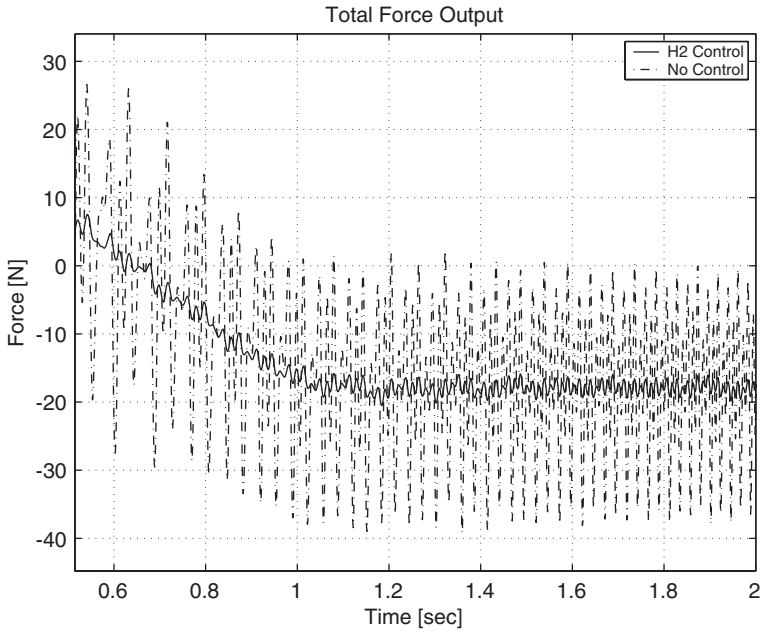

Fig. 11. Transmitted force at RHS due to a 4 s low nominal torque level acceleration from 700 to 5000 rev/min, with (solid) and without control (dash-dotted).

Even for some high nominal torque level disturbances with mounts and bushings forces within the linear stiffnesses ranges (e.g. due to rapid acceleration), the controller might require quite high actuator forces. Therefore, input saturation is likely to occur. To validate its effects, simulations have been carried out with actuators limited to ± 300 N. These simulations bring forward that input saturation is rather harmless for disturbances corresponding to driving operating conditions with low and moderate level nominal torque.

8. Concluding remarks

A MIMO controller for large frequency band attenuation of transmitted forces from the engine to chassis and body has been developed making use of $\mathscr{H}_2$ frequency domain-loop shaping technique, which showed to be powerful. The proposed solution deals with system nonlinearities and all possible engine disturbances except those corresponding to very high ramping speed or extremely high nominal engine torque (i.e. high values of α and L in Fig. 4) for which the controller has to be turned off.

The active engine suspension system design has been carried out making use of a virtual development environment for design, analysis, and co-simulation based closed-loop verification. This environment constitutes the foundation of a design strategy that facilitates dealing with dynamically complex plants. It is indicated that even for the fairly simple plant dynamic characteristics considered here, the possibility to perform realistic closed-loop system evaluations while covering all plant physical characteristics including nonlinearities is powerful.

Two different kinds of nonlinearities are shown to be lacking when the plant is linearised about engine static equilibrium position. Those are nonlinear material characteristics of the engine mounts and large angular engine displacements. To obtain desired performance and closed-loop stability, it is demonstrated that both nonlinearities have to be taken into account. This is done using gain scheduling with a low pass filtered form of the force transmitted to the body at LHS in the global x-direction as choice for scheduling parameter. Finally, it is clear that feedback control theory could be used when dealing with active engine vibration isolation systems.

Acknowledgements

This work has been carried out within Volvo Car Corporation's Post Graduate Program in association with Division of Automatic Control, Linköping University, Sweden.

Appendix A. Plant model data

The data given below are with respect to the global coordinate system.

A.1. Engine and torque rod model data

The engine mass (268.7 kg) centre of gravity is located at (1559.6, 41.4, 554.7) (mm), and the inertial properties, with respect to the centre of gravity, are (kg mm^2): I_{XX}: 23 960 000, I_{YY}: 11 330 000, I_{ZZ}: 24 040 000, I_{XY} : −800 000, I_{ZX}: 440 000, I_{YZ}: 2 340 000. The torque rod mass (0.13 kg) centre of gravity is located at (1872.0, −106.3, 315.0) (mm), and the inertial properties, with respect to the centre of gravity, are (kg mm^2): I_{XX}: 463.6, I_{YY}: 463.6, I_{ZZ}: 1.6, I_{XY}: 0.0, I_{ZX}: 0.0, I_{YZ}: 0.0.

A.2. Mounts and bushings stiffnesses and damping data

The location of the mounts and bushings are as follows $(x; y; z)$ (mm): LHS mount: (1606.0; −412.5; 725.0), RHS mount: (1510.4;476.9;778.7), TR front bushing: (1822.0; −107.5; 315.0), and TR rear bushing: (1510.4;476.9;778.7). The translational damping of the mounts and bushings are as follows $(x; y; z)$ (N s/mm): LHS mount: (0.1;0.1;0.15), RHS mount: (0.1;0.1;0.15), TR rear bushing: (0.1;0.1;0.15), TR front bushing: (0.15;0.15;0.15). The rotational damping of the mounts and bushings are as follows $(x; y; z)$ (N mm s/deg): LHS mount, RHS mount, and TR rear bushing: (0.0262;0.0279;0.0271), TR front bushing: (1.5;1.6;1.55).

The figures and data given below (Figs. A.1–A.4) present the nonlinear static stiffness characteristics of the mounts and bushings. Some stiffness characteristics are linear, these are: RHS mount

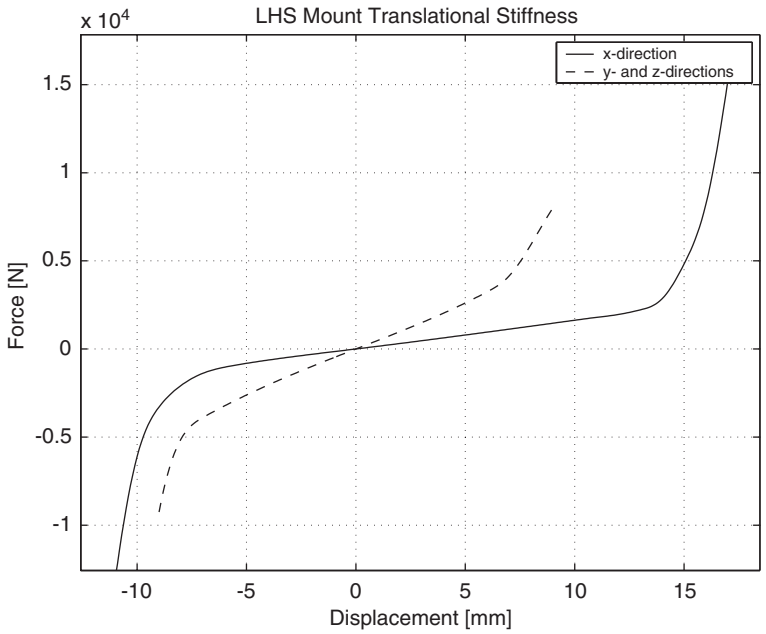

Fig. A.1. LHS mount static translational stiffnesses characteristics, in x- (solid), y- (dashed), and z-direction (dashed).

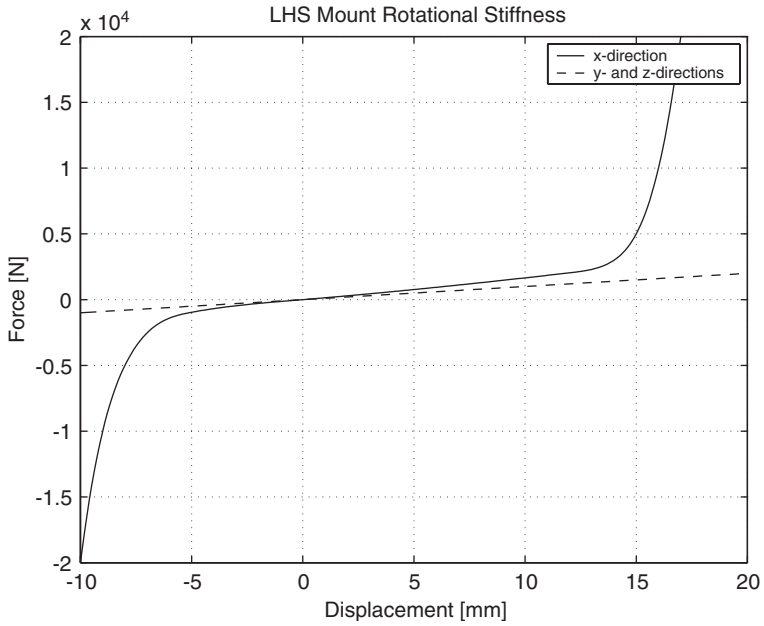

Fig. A.2. LHS mount static rotational stiffnesses characteristics, in x- (solid), y- (dashed), and z-direction (dashed).

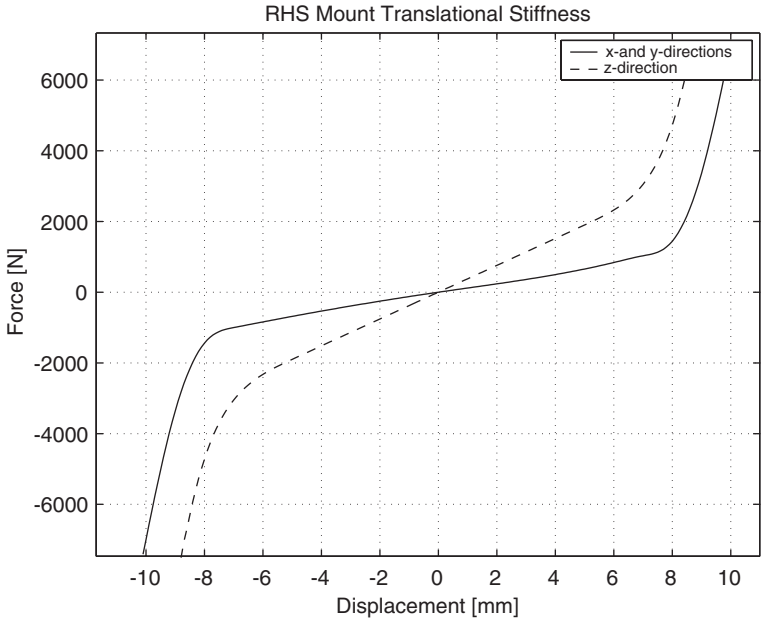

Fig. A.3. RHS mount static translational stiffnesses characteristics, in x- (solid), y- (solid), and z-direction (dashed).

rotational $(x; y; z)$:(0.1;0.1;0.1) (N m/deg), TR front bushing translational $(x; y; z)$: (10;10;10) (kN/mm), TR front bushing rotational $(x; y; z)$: (6;6;1) (N m/deg), and TR rear bushing rotational $(x; y; z)$: (0.01;0.01;0.01) (N m/deg).

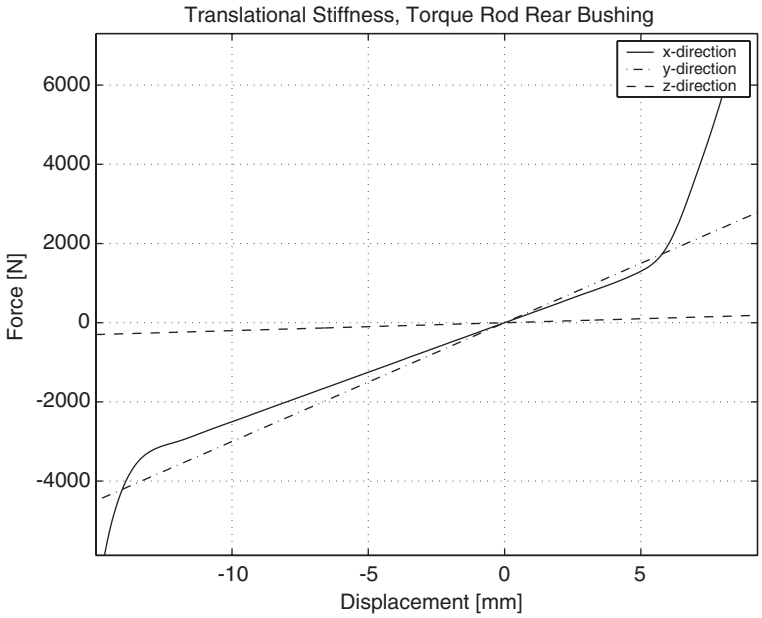

Fig. A.4. Torque rod rear bushing static translational stiffnesses characteristics, in x- (solid), y- (dash-dotted), and z-direction (dashed).

References

[1] A.M. McDonald, S.J. Elliott, M.A. Stokes, Active noise and vibration control within the automobile, in: *Proceedings of the International Symposium on Active Control of Sound and Vibration*, Acoustical Society of Japan, Tokyo, 1991.
[2] C.R. Fuller, S.J. Elliott, P.A. Nelson, *Active Control of Vibration*, Academic Press, New York, 1997.
[3] S.J. Elliott, I.M. Stothers, P.A. Nelson, A multiple error LMS algorithm and its application to the active control of sound and vibration, *IEEE Transactions on Acoustics, Speech, and Signal Processing* 35 (10) (1987).
[4] S.J. Elliott, C.C. Boucher, P.A. Nelson, The behaviour of a multiple channel active control system, *IEEE Transactions on Signal Processing* 40 (5) (1992).
[5] B. Widrow, S.D. Stearns, *Adaptive Signal Processing*, Prentice-Hall, Englewood Cliffs, NJ, 1985.
[6] T. Ushijima, S. Kumakawa, Active engine mount with piezo-actuator for vibration control, *Society of Automotive Engineers Paper 930201*, 1993.
[7] Y. Nakaji, S. Satoh, T. Kimura, T. Hamabe, Y. Akatsu, H. Kawazoe, Development of an active control engine mount system, *Vehicle System Dynamics* 32 (1999) 185–198.
[8] M. Muller, U. Weltin, D. Law, M.M. Roberts, T.W. Siebler, The effect of engine mounts on the noise and vibration behaviour of vehicles, SAE Technical Paper 940607, 1994.
[9] B.G. Watters, R.B. Coleman, G.L. Duckworth, E.F. Bukman, A perspective on an active machinery isolation, in: *Proceedings of the 27th Conference on Decision and Control*, Austin, Texas, 1988, pp. 2033–2038.
[10] J. Spanos, Z. Rahman, A. von Flotow, Active vibration isolation on an experimental flexible structure, in: *Proceedings of the SPIE North American Conference on Smart Structures and Intelligent Systems*, Albuquerque, New Mexico, SPIE, Vol. 1917, 1993, pp. 1917–1960.
[11] N. Tanaka, Y. Kikushima, Rigid support active vibration isolation, *Journal of Sound and Vibration* 125 (3) (1988).
[12] G.H. Blackwood, A.H. von Flotow, Active control for vibration isolation despite resonant base dynamics, *DSC-Vol.* 38, *Active Control of Noise and Vibration*, 1992.
[13] ADAMS, A registered trademark of Mechanical Dynamics Inc., 2301 Commonwealth Bouleward, Ann Arbour, Michigan 48105, USA.
[14] V.N. Sohoni, J. Whitesell, Automatic linearisation of constrained dynamical models, *Transactions of the ASME* 108 (1986).
[15] T. Glad, L. Ljung, *Control Theory—Multivariable and Nonlinear Methods*, Taylor and Francis, London and New York, 2000.
[16] K. Zhou, J.C. Doyle, K. Glover, *Robust and Optimal Control*, Prentice-Hall, Englewood Cliffs, NJ, 1996.
[17] J.C. Doyle, Guaranteed margins for LQG regulators, *IEEE Transactions on Automatic Control* 23 (4) (1978).
[18] K.J. Åström, T.B. Wittenmark, *Adaptive Control*, Addison-Wesley, Reading, MA, 1989.